Magnetic shielding properties of high-T_c superconducting hollow cylinders: Model combining experimental data for axial and transverse magnetic field configurations

J-F Fagnard[1], M Dirickx[1], M Ausloos[2], G Lousberg[3], B Vanderheyden[3] and Ph Vanderbemden[3]

[1] SUPRATECS, CISS Department, Royal Military Academy, B-1000 Brussels, Belgium
[2] SUPRATECS, University of Liège (B5), B-4000 Liege, Belgium
[3] SUPRATECS, University of Liège (B28), B-4000 Liege, Belgium

Abstract
Magnetic shielding efficiency was measured on high-T_c superconducting hollow cylinders subjected to either an axial or a transverse magnetic field in a large range of field sweep rates, dB_{app}/dt. The behaviour of the superconductor was modelled in order to reproduce the main features of the field penetration curves by using a minimum number of free parameters suitable for both magnetic field orientations. The field penetration measurements were carried out on Pb-doped Bi-2223 tubes at 77 K by applying linearly increasing magnetic fields with a constant sweep rate ranging between 10 μT/s and 10 mT/s for both directions of the applied magnetic field. The experimental curves of the internal field vs. the applied field, $B_{in}(B_{app})$, show that, at a given sweep rate, the magnetic field for which the penetration occurs, B_{lim}, is lower for the transverse configuration than for the axial configuration. A power law dependence with large exponent, *n'*, is found between B_{lim} and dB_{app}/dt. The values of *n'* are nearly the same for both configurations. We show that the main features of the curves $B_{in}(B_{app})$ can be reproduced using a simple *2-D* model based on the method of Brandt involving a $E(J)$ power law with an *n*-exponent and a field-dependent critical current density, $J_c(B)$, (following the Kim model: $J_c = J_{c0}\ (1+B/B_1)^{-1}$). In particular, a linear relationship between the measured *n'*-exponents and the *n*-exponent of the $E(J)$ power law is suggested by taking into account the field dependence of the critical current density. Differences between the axial and the transverse shielding properties can be simply attributed to demagnetizing fields.

1. Introduction

In a large frequency range, high temperature superconductors constitute magnetic screens with excellent shielding capabilities, and in particular at low frequency, their efficiency is higher than that of ferromagnetic materials [1-2]. Low magnetic field background is now necessary in various domains, such as magneto-encephalography where the utilization of SQUIDs (superconducting quantum interference device) is required [2-4]. Strong magnetic shielding is also needed in naval military applications, where the stray magnetic field of a vessel must be kept at a low level to avoid triggering influence mines [5].

Superconducting magnetic shields have the practical advantage of not requiring an *a priori* knowledge of the orientation of the magnetic field to be screened. However, for a shield of a given geometry, the attenuation factor may vary with the direction of the applied magnetic field. In particular, for cylindrical shields, it is essential to characterize the shielding efficiency for fields applied either parallel or perpendicular to the cylinder axis because of the importance of the demagnetizing field. In spite of numerous papers on this subject, there is no systematic study of the magnetic shielding properties of a superconducting tube combining *both* axial ($H \parallel$ axis of the tube) and transverse ($H \perp$ axis of the tube) directions of the applied magnetic field with several amplitudes

and frequencies (for AC fields) or with several sweep rates for the magnetic field (when the field is applied linearly).

Early experimental investigations of the magnetic shielding of superconducting tubes were carried by measuring the magnetic field inside a tube (either made of low-T_c or high-T_c material) subjected to an external magnetic field applied either axially or transversally. [6-7]. Models were then developed to describe the experimental observations.

In the *axial* configuration, the simplest model considered a cylinder of infinite extension and neglects magnetic relaxation effects. This approach led to a one-dimensional (*1-D*) critical state model [8] with either a constant or a field-dependent [9] critical current density J_c. This approach yielded simple analytical expressions, so that knowledge of the material parameters and the tube dimensions enabled all magnetic quantities to be predicted analytically. Conversely, the $J_c(B)$ dependence could be extracted from a fit to the experimental data [10]. Because of the neglect of magnetic relaxation phenomena, the critical state yielded frequency independent results [11-13]. In high-T_c superconductors, at the boiling point of nitrogen, the frequency (or sweep rate) dependence of the magnetic properties could be taken into account by means of a non-linear *E-J* constitutive law ($E \propto J^n$) with a large exponent, *n*. With this law and for a *1-D* cylindrical geometry, the diffusion equation of magnetic flux was solved and the frequency dependence of the magnetic properties was determined by using scaling laws [14]. The advantage of using a continuous $E \propto J^n$ law is that it can be incorporated into a suitable *2-D* model to investigate the finite-size effects in the axial configuration of a cylinder with a finite height. The magnetic properties could be predicted using either the semi-analytical approach developed by Brandt [14-15] or other numerical methods such as finite element methods [16-23], Monte-Carlo method [24] or variational principles [25]. In our previous work [26], we used the Brandt algorithm to study the competition between two mechanisms of field penetration in the tube (from the lateral surface and through the opening ends) and we used scaling laws to explain the frequency-dependence of the magnetic shielding performances [10, 26].

In the transverse configuration, the simplest approach to calculate the shielding efficiency involves a *2-D* model: the tube was assumed to be infinitely long in the *z* direction and variables of integration are function of both the radial distance (r) and the angular position (θ) from the direction of the transverse magnetic field (referenced at $\theta = 0°$). In the framework of the critical-state model with field-independent J_c, analytical expressions of the field distribution in a bulk cylindrical wire subjected to a transverse field [27] showed that the penetration is initiated at the angles $\theta = \pm\pi/2$ where the net magnetic field is maximal. At these angular positions, the local magnetic field at the outer edge of the tube is twice the applied magnetic field because of the demagnetizing factor $D = 1/2$. For weak penetration and assuming a field-independent J_c, the penetration depth of the magnetic flux in the cross section of the cylinder varied as $\sin\theta$ [27]. The penetration of a transverse field into a hollow superconducting cylinder was studied by Zolotovitskii et al. within a critical state model with a field-dependent $J_c(B)$ [28] (results were compared to the data assuming a $J_c(B)$ dependence with two possible values only, i.e. $J_c = J_0$ and $J_c = 0$ for $B > B_0$). A phenomenological "shell" model was also suggested by Zhilichev [29-30] in order to predict the hysteresis and losses in a superconducting tube. In addition to the approaches based on the critical state, models using a $E \propto J^n$ constitutive law were also used to predict the frequency dependence of the transverse field penetration in bulk cylinders, either via the semi-analytical algorithm developed by Brandt [14-15] or by means of a finite-element model [31-32]. On the basis of a flux-flow model, Matsuba et al. investigated the axial and transverse flux penetration in Bi-2212 tubes [33], but their experimental results did not point out any frequency dependence of the magnetic shielding properties.

More complex approaches were also developed. Mikitik and Brandt extended the critical-state theory to non symmetric samples and in the case of a magnetic field applied along a direction which does not correspond to a symmetry axis [34]. Karmakar and Bhagwat presented a theoretical formulation of the critical state model for infinite cylindrical samples subjected to a magnetic field in an arbitrary direction [35]. In spite of the number of literature results mentioned above, there is no systematic explanation of the experimental data from modelling results for magnetic shielding by means of a superconducting tube for *both* axial and transverse directions, with a model that accounts for the frequency (or sweep rate) dependence.

The aim of the present work is twofold. First, we aim at describing a method to characterize superconducting magnetic screens by determining the superconducting properties of a hollow cylinder with the *minimum* number of free parameters that are necessary to correlate the modelled curves and the experimental data on HTS tubes at 77 K. For that purpose, measurements of magnetic field penetration will be performed for both axial and transverse magnetic fields and will be compared to theoretical predictions obtained either by *1-D* critical state expressions (axial configuration) or through the *2-D* Brandt algorithm (axial and transverse configurations).

Second, the numerical simulations are used to investigate the effects of (i) the field dependence of the critical current density, (ii) the non-linearity of the $E(J)$ relationship, and to identify their signature on the flux penetration curves.

The paper is structured as follows. In section 2, we introduce the theoretical framework for the numerical simulations and the constitutive laws ruling the superconducting properties. In section 3, the experimental setup is briefly described. The section 4 is devoted to the description of the experimental results. We discuss simulation results in section 5. In a first subsection, calculations are carried out for field-dependent and field-independent critical current densities in order to point out the role played by the laws $E(J)$ and $J_c(B)$ on the frequency response of the superconducting shield. Then, on the basis of these results, we suggest a method to extract the parameters of the two constitutive laws in the particular case of the sample measured in section 4. A third subsection deals with the flux penetration processes by considering the effect of the demagnetizing factor and the field dependence of the critical current density. Several cases will be discussed regarding the given geometry and the flux profiles within the superconducting thickness.

2. Theoretical framework

In order to study the penetration of a magnetic field in a superconducting hollow cylinder, we use a numerical model based on the Brandt algorithm [14-15]. This model has been used for predicting the magnetic properties of long thin strips and circular disks in a perpendicular magnetic field [14], for circular disks of arbitrary thickness and cylinders of finite length subjected to an axial magnetic field [15], and for superconducting tubes subjected to an axial magnetic field [26, 36]. The method is based on the discretization and on the numerical integration of the Biot-Savart equations in order to determine the current density $\boldsymbol{J}(\boldsymbol{r}, t)$ inside the volume of the superconductor. The magnetic flux density inside the superconducting tube is then calculated from the current density distribution.

The general form of the equation of motion for J, inside the volume of the superconducting tube subjected to either axial or transverse magnetic field, can be written as

$$\dot{J}(\boldsymbol{r},t) = \frac{1}{\mu_0}\int_{\Omega} \mathrm{d}\boldsymbol{r}' Q^{-1}(\boldsymbol{r},\boldsymbol{r}')\left\{E\left[J(\boldsymbol{r}',t)\right] - E_{\mathrm{app}}(t)\right\}. \tag{1}$$

In the *axial magnetic field configuration* (figure 1a), we consider a type II superconducting hollow cylinder of inner radius a_1, outer radius a_2, and height l along the z-axis. The coordinates are $\boldsymbol{r} = (r, z)$, $\boldsymbol{r}' = (r', z')$ and the integration is performed between $r = a_1$ and $r = a_2$, and between $z = 0$ and $z = l/2$. The integral kernel can be written as explained in [14]:

$$Q(\boldsymbol{r},\boldsymbol{r}') = f(r,r',z-z') + f(r,r',z+z') \tag{2}$$

$$\text{with} \qquad f(r,r',\eta) = \frac{1}{2\pi}\int_0^{\pi} \frac{r'\cos\varphi \,\mathrm{d}\varphi}{\left(\eta^2 + r^2 + r'^2 + 2rr'\cos\varphi\right)^{1/2}}, \tag{3}$$

$$\text{and} \qquad E_{\mathrm{app}}(t) = \frac{r'}{2}\dot{B}_{\mathrm{app}}. \tag{4}$$

In the *transverse magnetic field configuration* (figure 1b), the tube is considered to be infinitely long. The integration variables are $\boldsymbol{r} = (x, y)$, $\boldsymbol{r}' = (x', y')$ and the integration is done over the cross-section of the tube. The integral kernel is now written as [15]:

$$Q(\boldsymbol{r},\boldsymbol{r}') = \frac{\ln|\boldsymbol{r}-\boldsymbol{r}'|}{2\pi} \tag{5}$$

$$\text{and} \qquad E_{\mathrm{app}}(t) = x'\dot{B}_{\mathrm{app}}. \tag{6}$$

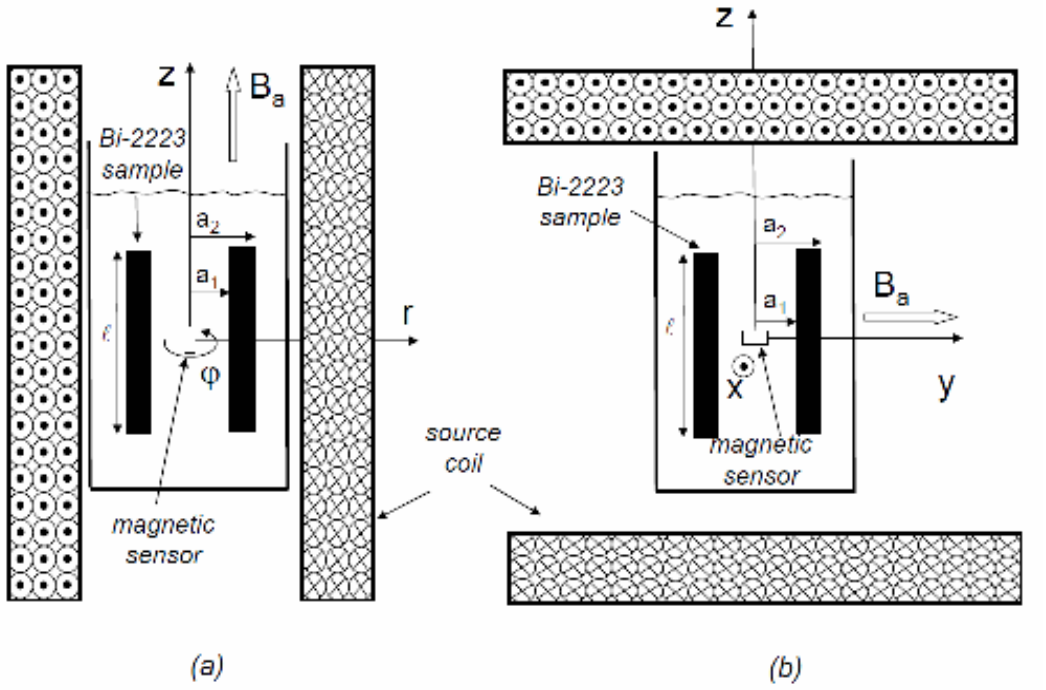

Figure 1. Schematics of the experimental setup for axial and transverse magnetic field configurations.

The electric field is expressed in term of J by using the material constitutive law $\boldsymbol{E}(\boldsymbol{J})$. In order to take the flux creep effect into account, we use the power-law:

$$E(J) = E_c\,(J/J_c)^n, \tag{7}$$

where E_c and J_c are the critical values of the electric field and the current density.

We aim at modelling the flux penetration in a polycrystalline Bi-2223 bulk material for which the critical current density is strongly field-dependent. In this work, we use the Kim model [37]:

$$J_c(B) = J_{c0}\,(1+ B/B_1)^{-1} \tag{8}$$

where J_{c0} and B_1 are determined by fits on the experimental $J_c(B)$.

Equation of motion (4) is discretized on a *2-D* grid and solved iteratively from $J_i(t=0) = 0$. Then, we obtain $J_i(t+\mathrm{d}t) = J_i(t) + \dot{J}_i(t)dt$ using a variable time step dt in order to increase the stability and the speed of the computation. Details on the numerical aspects of the method are discussed in [14-15].

3. Experimental setup

In this work, we use a Pb-doped Bi-2223 polycrystalline hollow cylinder from CAN Superconductors that has an inner diameter a_1 of 12 mm, a wall thickness (a_2 - a_1) of 1.6 mm, and a length l of 80 mm.

Magnetic measurements are performed in a liquid nitrogen bath (T = 77 K) under zero field cooled conditions. The copper coil generating the magnetic field is such that the sample can be placed with its axis either parallel or perpendicular to the coil axis. The setup is shown in figure 1, for both the axial and transverse configurations. The copper coil is fed by a current of maximum amplitude of 10 A (HP6030A DC power supply), corresponding to an applied magnetic field at the centre of the coil, of $\mu_0 H_{app}$ = 36 mT. The dimensions of the coil are large enough to ensure homogeneity of the applied magnetic field, with relative variations less than 1.5% along the axis of the cylinder [38]. In order to increase the sensitivity of the magnetic field measurement and to protect the experiment against stray magnetic fields, the setup is placed inside two concentric mu-metal ferromagnetic enclosures.

The magnetic flux density at the centre of the superconducting tube, B_{in}, is measured by a high sensitivity Hall probe (Arepoc HHP-MP). The probe is always oriented along the applied magnetic field, for both axial and transverse configurations. The Hall probe voltage is sampled at a rate of 20 samples/s by a PCI-6221 National Instrument Data Acquisition Card (DAQ) after being amplified and filtered.

The waveform of the applied magnetic field, $B_{app}(t)$, is computed by a user Labview® interface. In this work we will only discuss experiments performed under a constant sweep rate of the magnetic field. The interface allows us to increase the magnetic field from 0 to 16 mT with well-defined sweep rates, dB_{app}/dt, ranging between 10 µT/s and 10 mT/s.

4. Experimental results

In a first set of measurements, the sample is placed in the axial magnetic field configuration. The field penetration measurements carried out at $dB_{app}/dt = 10$ µT/s, 100 µT/s, and 1 mT/s are plotted in figure 2. It can be observed that at low increasing fields starting from $B_{app} = 0$ mT, the internal flux density at the centre of the tube, B_{in}, is significantly below the applied magnetic field, as the magnetic shielding of the superconductor is effective. The shielding factor, SF, defined as the ratio of B_{app} over B_{in} is high at low B_{app} and decreases as the applied magnetic field increases. Above a given value of B_{app}, the magnetic field starts to enter the hollow of the tube and B_{in} increases. We define B_{lim} as the threshold value of the applied magnetic flux density for which the shielding factor drops below a fixed level, which we arbitrarily choose to be equal to 1000. This gives $B_{lim} \approx 14.1$ mT and 8.4 mT in axial and transverse configurations for a sweep rate of 1 mT/s. As can be seen in figure 2, the curve $B_{in}(B_{app})$ shifts to the right as dB_{app}/dt increases. Thus, B_{lim} increases by 11 % when the magnetic field sweep rate dB_{app}/dt is increased by a factor of 100.

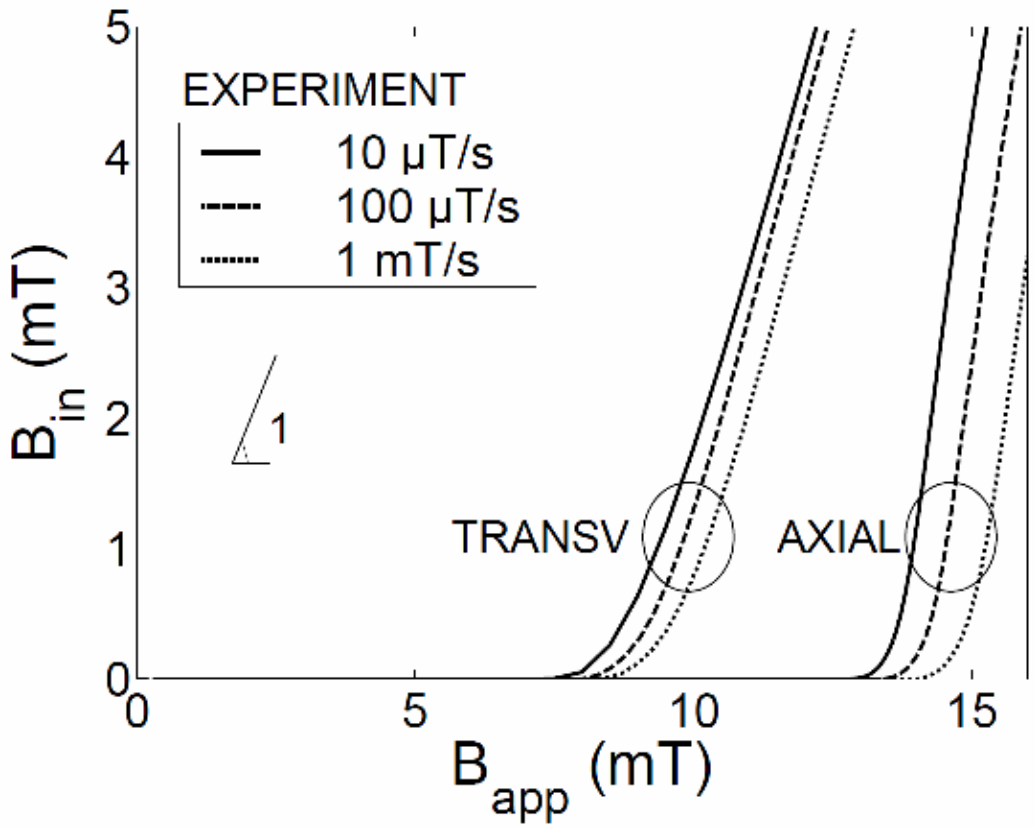

Figure 2: Experimental results of $B_{in}(B_{app})$ for several sweep rates, $dB_{app}/dt = 10$ µT/s, 100 µT/s and 1 mT/s, in the axial and the transverse configurations.

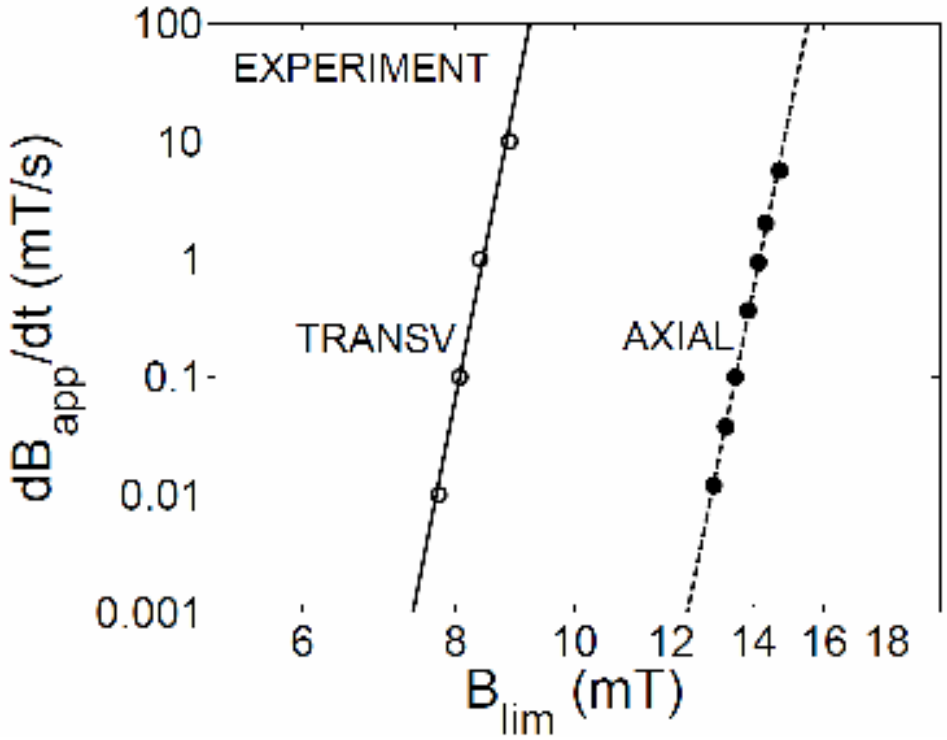

Figure 3. Double logarithmic plot of dB_{app}/dt as a function of B_{lim}, in the axial and the transverse configurations (experimental results).

A second set of experiments is performed in the transverse magnetic field configuration. The results (figure 2) show that the magnetic field enters the superconducting tube for smaller values of the applied magnetic field than in the axial configuration. Similarly to the axial magnetic field configuration, the curve $B_{in}(B_{app})$ shifts to the right for increasing dB_{app}/dt. Compared with the value obtained for a magnetic field sweep rate $dB_{app}/dt = 10$ μT/s, B_{lim} increases by 8 % when the measurement is carried out at $dB_{app}/dt = 1$ mT/s. The slopes of the field penetration curves $B_{in}(B_{app})$ in the transverse magnetic field configuration are lower than those in the axial magnetic field configuration.

The values of dB_{app}/dt are plotted in figure 3 as a function of B_{lim}, on a double logarithmic scaled graph for both axial and transverse magnetic field configurations. It can be observed that the measured data points are aligned over several decades. We can reasonably infer a power law dependence with an exponent labelled *n'*, to distinguish it from the *n* exponent of the constitutive law $\boldsymbol{E}(\boldsymbol{J})$. Here, *n'* is equal to 50.6 for the axial magnetic field configuration and 52.3 for the transverse magnetic field configuration.

5. Numerical results and discussion

5.1. Combined effects of the constitutive laws E(J) and $J_c(B)$

With a view to comparing experimental and numerical results, some prior calculations are needed to highlight the difference and to find a link between the exponents *n* and *n'*, which are respectively characteristic of the $E(J)$ power law and of the measured power law relating dB_{app}/dt and B_{lim}. Consider the constitutive law $E = E_c (J/J_c)^n$. In a given range of magnetic fields, Kim's law, that expresses the magnetic field dependence of J_c, can be approximated by a negative power law, $J_c = J^*(B/B^*)^{-\gamma}$. Note that the values of J^*, B^* and γ slightly depend on the particular magnetic field range used for the approximation. The chosen range is 5 mT to 20 mT in order to avoid the divergence at the origin and to include the values of B_{lim} in both axial and transverse configurations. With such a dependence, the $E(J)$ power law becomes:

$$\begin{aligned} E &= E_c J^n / (J^*(B/B^*)^{-\gamma})^n \\ &= E_c [B^{*-\gamma n}/J^{*n}] B^{\gamma n} J^n. \end{aligned} \quad (9)$$

If the average magnetic flux density in the superconductor, $\langle B \rangle$, is assumed to be proportional to the average current density flowing in the cylinder, $\langle J \rangle$, and if the current density variations are neglected to first order, then the relationship between the electric field and the current density can be approximately described as $\langle E \rangle \propto \langle J \rangle^{n.(1+\gamma)}$ [19].

Consequently, as $-\mathrm{d}\boldsymbol{B}/\mathrm{d}t = \nabla \times \boldsymbol{E}$ and B_{lim} is proportional to the average current density that can flow in the superconductor, the relationship between $\mathrm{d}B_{\mathrm{app}}/\mathrm{d}t$ and B_{lim} should correspond, at first order (if we consider that $\mathrm{d}B_{\mathrm{app}}/\mathrm{d}t$ varies in the same way as $\mathrm{d}B/\mathrm{d}t$), to a power law dependence with an exponent $n' = n\,(1+\gamma)$.

In order to verify the validity of this result, simulations with different magnetic field dependences of J_c are executed. First we implement the case $\gamma = 0$ that corresponds to a field-independent critical current density, with $J_c = J_{c0} = J^*$, where J_{c0} is fixed to 1000 A/cm². We compute simulations for $\mathrm{d}B_{\mathrm{app}}/\mathrm{d}t$ ranging between 10 µT/s and 10 mT/s with a n-value of 30 (this is a characteristic value for HTS polygranular samples of Bi-2223 at 77 K and in the low magnetic field regime [19, 26, 39]). A comparison between the two configurations at a fixed sweep rate ($\mathrm{d}B_{\mathrm{app}}/\mathrm{d}t$ = 1 mT/s) leads to two observations.

First, B_{lim} in the axial configuration is larger than in the transverse configuration by a factor of 1.85 (figure 4). This result is consistent with the factor of two that is expected from the demagnetization effects in the limit of an infinitely long tube of circular cross-section (for which the demagnetizing factor, D, equals ½). In the present case, however, the finite length of the tube and the detailed field distribution inside the tube reduce this factor to 1.85. A second observation is that, for applied magnetic fields of a few mT above B_{lim}, the internal magnetic field increases linearly with the applied magnetic field, in both the axial and the transverse configurations, with an equal slope. For both configurations, the values of $\mathrm{d}B_{\mathrm{app}}/\mathrm{d}t$ are plotted as a function of B_{lim} on a double logarithmic scaled graph (figure 5). The fit of these data leads to a power exponent, n', equal to 28.3 for the transverse configuration and 31.2 for the axial configuration. These values are very close to the n-value used in the modelling (n = 30).

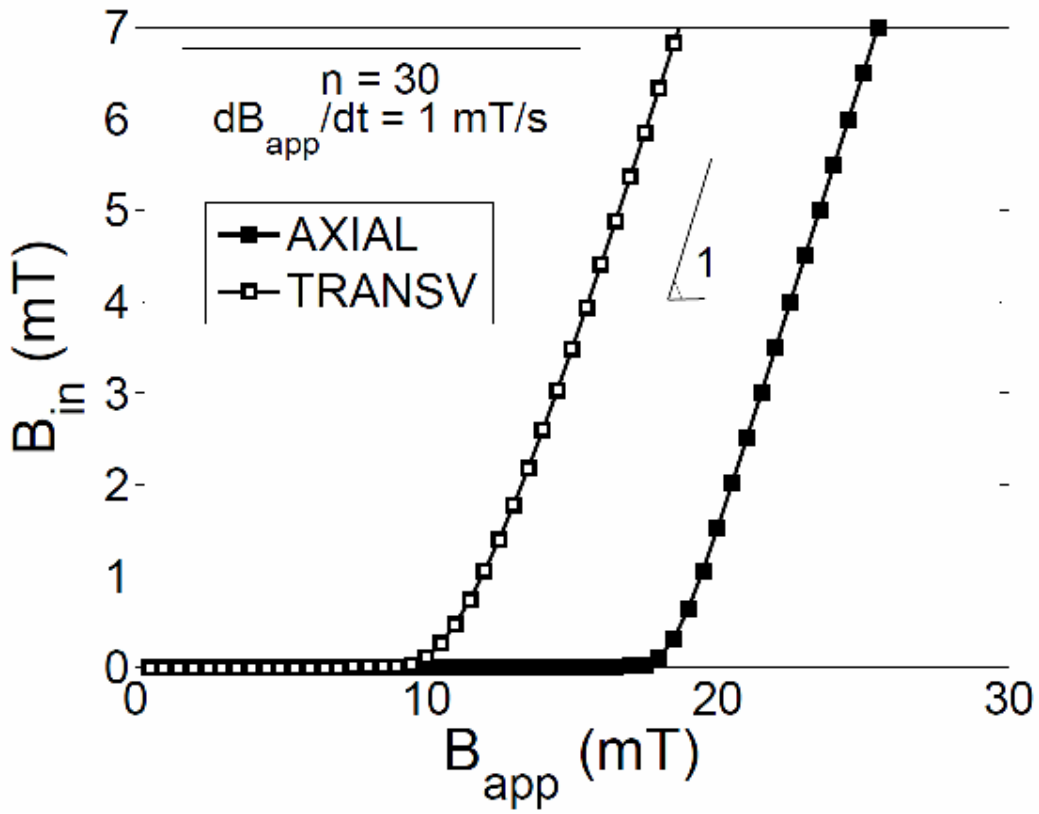

Figure 4. Modelling results of $B_{\mathrm{in}}(B_{\mathrm{app}})$ at $\mathrm{d}B_{\mathrm{app}}/\mathrm{d}t$ = 1 mT/s for a field-independent $J_c = J_{c0}$ = 1000 A/cm² and n = 30 in axial configuration and in transverse configuration.

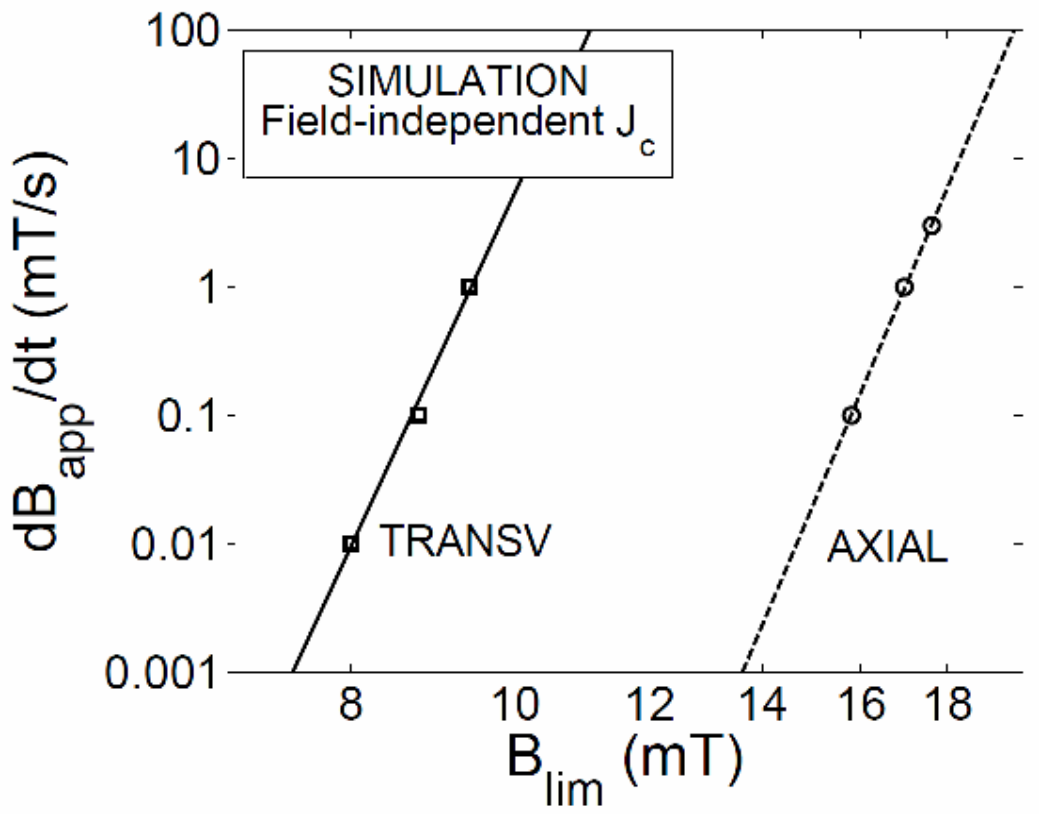

Figure 5. Double logarithmic plot of dB_{app}/dt as a function of B_{lim} extracted from simulations in axial and transverse configurations with a field-independent $J_c = J_{c0} = 1000$ A/cm² and $n = 30$.

A second set of simulations is carried out for the same values of dB_{app}/dt and $n = 30$, but now with a field-dependent J_c. Here, the critical current density is implemented with the Kim model using $J_{c0} = 4000$ A/cm² and $B_1 = 2$, 4 and 8 mT. Because of the strong field dependence of the critical current with these parameters, the value of J_{c0} is chosen four times larger than that used in the field-independent J_c case in order to obtain a B_{lim} of the same order of magnitude. The fits of the corresponding $dB_{app}/dt(B_{lim})$ relationships plotted in a double logarithmic graph give power law exponents n' respectively equal to 46.7, 49 and 52.5. In order to be compared with the theoretical values of $n' = n(1+\gamma)$, the Kim model can be approximated, if $dB_{app}/dt \in$ [5 mT, 20 mT], by using the power law with a negative exponent, $-\gamma$. The fits of the curves for $B_1 = 2$, 4 and 8 mT give respectively $\gamma = 0.83$, 0.72 and 0.56. The comparison between computed and theoretical values is presented in figure 6. We conclude that numerical results for the axial and the transverse magnetic configurations are in agreement with the simple theory combining $\boldsymbol{E}(\boldsymbol{J})$ power law and field-dependent J_c. These simulations confirm the fact that the relationship between n and n' is to be attributed to the field dependence of the critical current density.

5.2. Determination of the constitutive law parameters

In this section, we present a method that allows one to extract the material parameters (J_{c0}, B_1, n) of a given superconducting tube, from a minimal number of simulation fits to experimental data. The procedure starts with an "educated guess" for the initial parameters (J_{c0}^{init}, B_1^{init} and n^{init}) as obtained from a simple one-dimensional critical state model where we consider a field-dependent J_c.

The initial parameters for the simulations of the flux penetration are (i) a n^{init}-value equal to 30 (typical value for HTS at 77 K) and (ii) the initial parameters of the Kim model (J_{c0}^{init}, B_1^{init}) deduced from the simple *1-D* critical state model. The model assumes an infinitely long hollow tube subjected to an axial magnetic field with a field-dependent J_c following the Kim law. In this framework, it can be shown [10] that the magnetic field at the centre of the tube, B_{in}, equals zero below

$$B_{lim} = -B_1 + \sqrt{B_1^2 + 2d\mu_0 J_{c0} B_1}\ . \qquad (10)$$

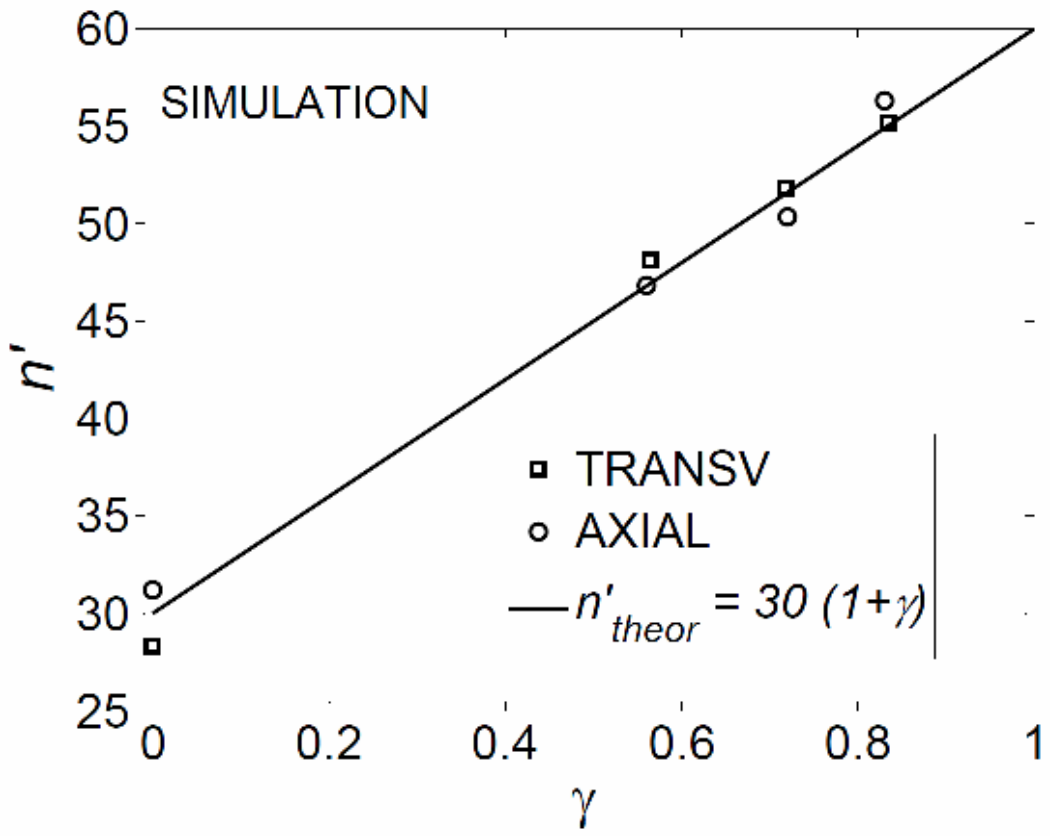

Figure 6. Comparison between the theoretical values $n' = n\,(1+\gamma)$ with n = 30 and the n'-value from fits of $dB_{app}/dt(B_{lim})$ obtained with a field-dependent J_c following the Kim model using J_{c0} = 40 MA/m² and B_1 = 2, 4 and 8 mT giving power law approximations with respectively γ = 0.83, 0.72 and 0.56 and a field-independent J_c (γ = 0).

Above this value, B_{in} equals

$$B_{in} = -B_1 + \sqrt{\left(B_1 + B_{app}\right)^2 - 2d\mu_0 J_{c0} B_1}\ . \tag{11}$$

If we consider a linearly increasing magnetic field up to B_{max}, we define $B_{int,max}$ as the internal magnetic flux density at this maximum value. The Kim law parameters can be deduced from the measurements of $B_{int,max}$, B_{max} and B_{lim} at a sweep rate that is chosen in the interval used in the experiment (i.e. between 10 µT/s and 10 mT/s here). It is important to notice that the *1-D* model does not take into account the dependence of B_{lim} with respect to dB_{app}/dt. The formulas giving the Kim law parameters (J_{c0}, B_1) are [10]:

$$B_1^{\,init} = \frac{1}{2}\frac{(B_{lim}^2 + B_{int,max}^2 - B_{max}^2)}{(B_{max} - B_{lim} - B_{int,max})} \tag{12}$$

$$J_{c0}^{\,init} = \frac{B_{lim}}{d\mu_0}\left(1 + \frac{B_{lim}}{2B_1}\right) \tag{13}$$

When considering the $B_{in}(B_{app})$ measurements carried out at 100 µT/s in the axial configuration, we have B_{max} = 15.9 mT, $B_{int,max}$ = 5 mT and B_{lim} = 13.54 mT, so this gives $J_{c0}^{\,init}$ = 1215 A/cm² and $B_1^{\,init}$ = 8.4 mT. Next, once these initial parameters ($J_{c0}^{\,init}$, $B_1^{\,init}$ and n^{init}) are determined, simulations are performed in the axial and the transverse magnetic field configurations at 10 µT/s, 100µT/s and 1 mT/s, and B_{lim} is determined for each curve $B_{in}(B_{app})$. The n'-values are determined from the curve $dB_{app}/dt(B_{lim})$ extracted from measurements (figure 3) and from the simulation results, and are then compared. Then, n^{init} is adjusted in the simulation code in order to have the best concordance of the slopes of the curves $dB_{app}/dt(B_{lim})$ on a log-log plot showing experimental

and simulation results (i.e. *n'*-values). The resulting value is chosen as the *n*-value used in the constitutive ***E***(***J***) law.

The next step is to obtain the correct parameters for the law $J_c(B)$ (J_{c0} and B_1). In the range of magnetic field where shielding occurs, no information can be obtained from a fit. So, we focus on the curves $B_{in}(B_{app})$ above B_{lim} in transverse and in axial magnetic field configurations. We showed earlier that for a field-independent J_c, the slope of the curve $B_{in}(B_{app})$ in an axial configuration is the same as in the transverse configuration (figure 4). The difference between the slopes of the curves $B_{in}(B_{app})$ is thus attributed to the magnetic field dependence of the critical current density. From the Kim model, it can be seen that for $B >> B_1$, the critical current density tends to $J_c = J_{c0}\, B_1 / B$. So, keeping the product $J_{c0}\, B_1$ close to the product $J_{c0}^{init}\, B_1^{init}$, the aim is to find the parameters that gives the best agreement between measured and computed slopes of the $B_{in}(B_{app})$ curves in the transverse and the axial magnetic field configurations.

The as-obtained numerical results with $J_{c0} = 4000$ A/cm², $B_1 = 2$ mT and $n = 29$ are presented in figure 7. In the same figure, we plot the magnetic field calculated by using the analytical formula (11) established with the critical state model with a field-dependent critical current density following the Kim law. Because of the definition of the critical current density for a critical electric field equal to 1 µV/cm, the Faraday law implies that the characteristic dB/dt to be considered at a radius equal to a_2 is equal to 26 mT/s. It can be seen on the figure that the location of the Bean-Kim curve (dashed-dot line) is consistent with the simulation results at lower ranging rates. The non-linear $E(J)$ relationship is responsible for the positive curvature of the simulated curves, in contrast to the Bean-Kim curve which displays a negative curvature.

Figure 8 shows dB_{app}/dt as a function of B_{lim} (on a double logarithmic scale) for the final set of parameters J_{c0}, B_1, and n. In this axis system the data points are aligned and, as for the experimental results, we can infer a power law dependence with an exponent n' equal to 52.5 for the axial magnetic field configuration and to 52.1 for the transverse magnetic field configuration.

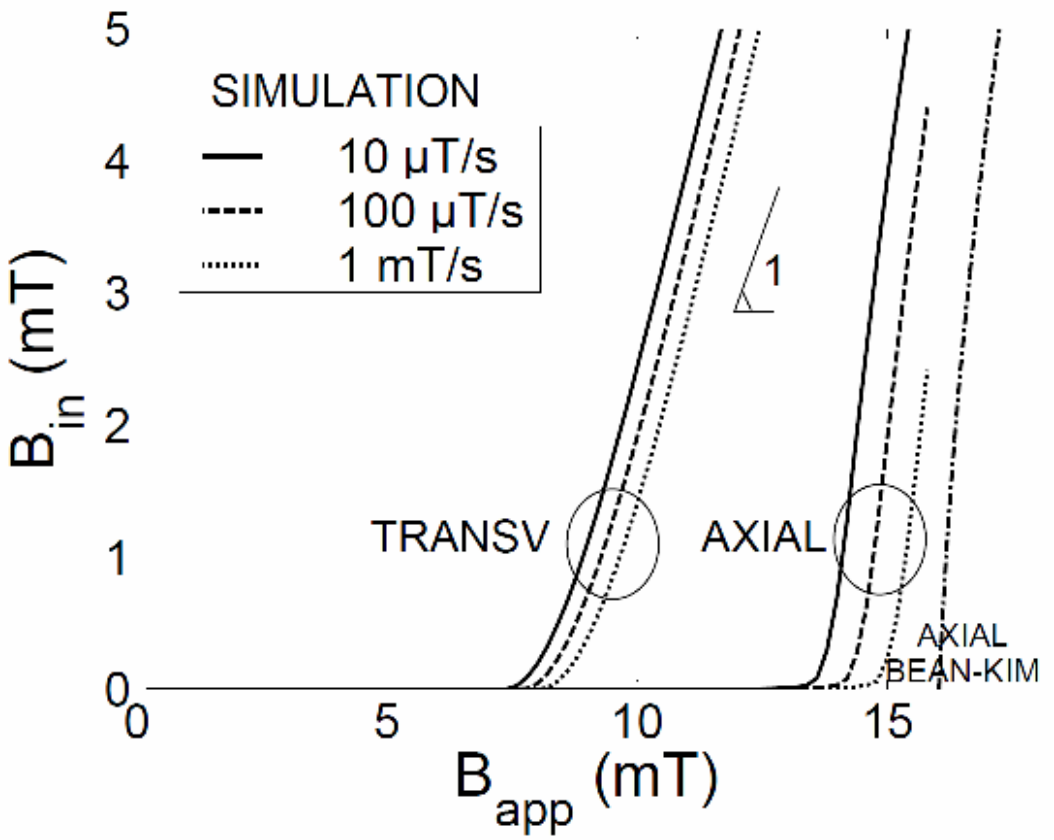

Figure 7. Modelling results of $B_{in}(B_{app})$ for several sweep rates, dB_{app}/dt = 10 µT/s, 100 µT/s and 1 mT/s, in axial configuration and in transverse configuration. Analytical curve $B_{in}(B_{app})$ using the Bean model and the Kim law for an infinitely long tube of same cross-section subjected to an axial magnetic field.

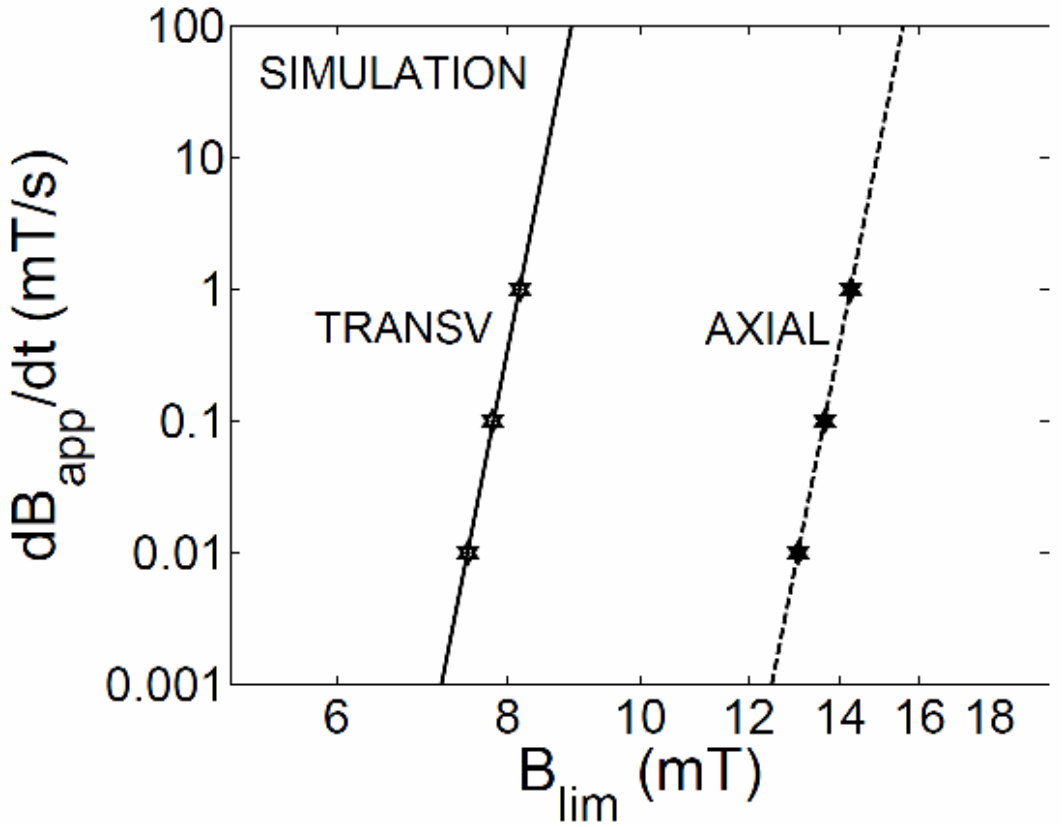

Figure 8. Double logarithmic plot of dB_{app}/dt as a function of B_{lim} in axial and transverse configurations (simulation results).

It can be checked that these values nicely agree with those obtained from the experimental results (figure 3). In addition, the *n'*-values for the axial and the transverse magnetic field configurations are quite close to each other. This observation makes sense given the fact that both the critical current density and the $E(J)$ law are assumed to be isotropic.

5.3. Discussion on the flux penetration processes

In this subsection, we compare the penetration of the magnetic flux for both axial and transverse magnetic fields with either constant or field-dependent J_c. The simulations are quite helpful to understand these processes as it is possible to calculate the magnetic field at any point of the space. In particular, for the axial configuration, the locations of interest are in the medium plane of the cylinder for radii equal to 0, a_1 (inner radius) and a_2 (outer radius).

In the case of a constant critical current density, when the magnetic field is axial, the flux penetration does not depend on the azimuthal angle θ and the demagnetizing factor, D, for our long sample of finite height is equal to 0.05 ($D = 0$ would correspond to an infinitely long tube). As a consequence, the magnetic field at the outer radius of the superconducting tube increases linearly with the applied magnetic field (figure 9), i.e.

$$B_{outer} = (1-D)^{-1} B_{app}. \quad (14)$$

For the transverse configuration, we are interested in the local magnetic field at the points located along a diameter perpendicular to the applied magnetic field direction (x direction) at the radii $r = 0$ (point A), $r = a_1$ (point B), and $r = a_2$ (point C) (inset of the figure 10).

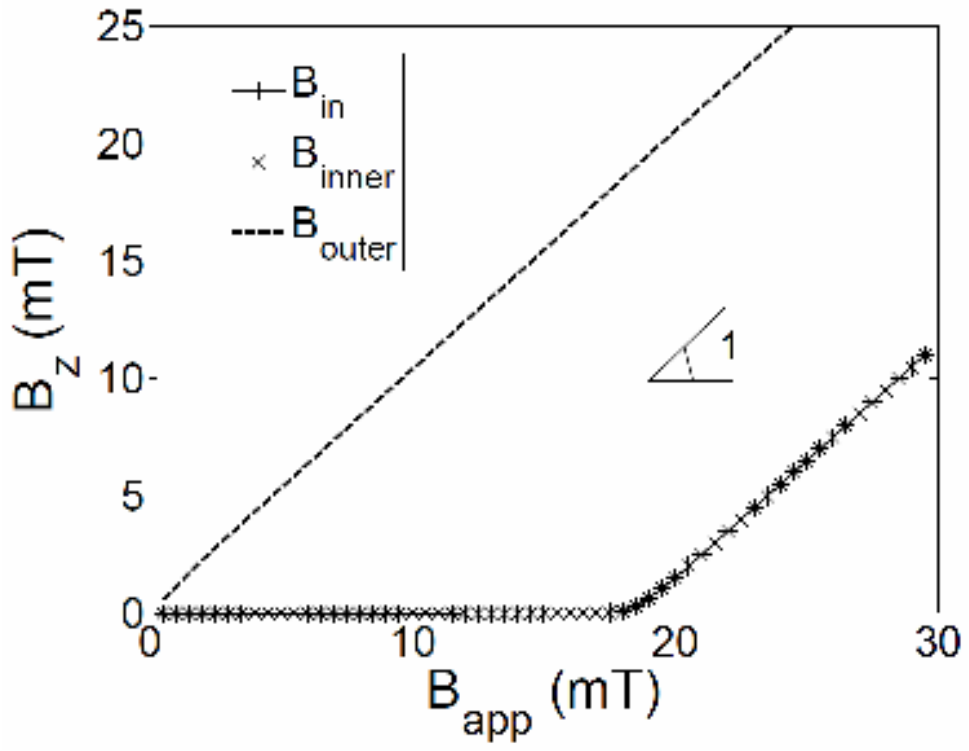

Figure 9. Axial component of the local magnetic flux density, B_z, in function of the applied magnetic field at the centre of the cylinder (B_{in}), at the inner radius of the cylinder (B_{inner}) and at the outer radius of the cylinder (B_{outer}) for a constant J_c = 1000 A/cm² and in the axial magnetic field configuration.

By contrast, for a transverse magnetic field, the demagnetizing factor has a strong influence on the magnetic field distribution around the tube. Calculations of this demagnetizing factor have been summarized for several geometries such as general ellipsoids [40], cylinders [41] or thin disks [42]. Indeed, the demagnetizing factor of an infinite cylinder with a circular cross-section in the transverse direction is equal to ½, so that the applied magnetic field at the outer diameter along the y direction (point C) equals twice the applied magnetic field, whereas it vanishes at the outer diameter along the x direction (point D) as it can be seen on the inset of the figure 10 for an applied magnetic field equal to $\mu_0 H_{app}$ = 6.6 mT. As soon as the magnetic field penetrates the wall, the flux front has an elliptical shape because the magnetic field at the outer radius is not independent on θ. This modification of the flux profile implies that the demagnetizing factor is no longer equal to 1/2 but has to be close to that of a cylinder with an elliptic cross-section [40]. In particular, at B_{lim}, the superconductor is fully penetrated along the perpendicular direction, whereas the magnetic field has barely penetrated along the applied magnetic field direction. For this value of the applied magnetic field, we may evaluate the demagnetizing factor by considering an infinite cylinder with an elliptic cross-section with the small axis equal to a_1 in the direction orthogonal to the magnetic field direction and a large axis a_2 in the applied field direction. According to the dimensions of the hollow cylinder studied in this work, the demagnetizing factor is equal to

$$a_2/(a_1+a_2) = 0.56 \quad (15)$$

in the transverse direction and to

$$a_1/(a_1+a_2) = 0.44 \quad (16)$$

in the direction of the applied magnetic field. This gives a value of the applied magnetic field at the point C equal to 1.79 times the applied magnetic field.

In the figure 10, it can be seen that the magnetic field at point C, B_{outer}, increases twice as fast as the applied magnetic field for low values, and then increases with a decreasing rate until $B_{app} = B_{lim}$. Note that for B_{app} = 10 mT the outer magnetic field is equal to 17.38 mT, a value which is close to the value of 17. 85 mT calculated from equations (14) and (16). These demagnetization effects, leading to the magnification of the local magnetic field at point C, are responsible for the fact that B_{lim} is lower in the transverse configuration than in the axial configuration.

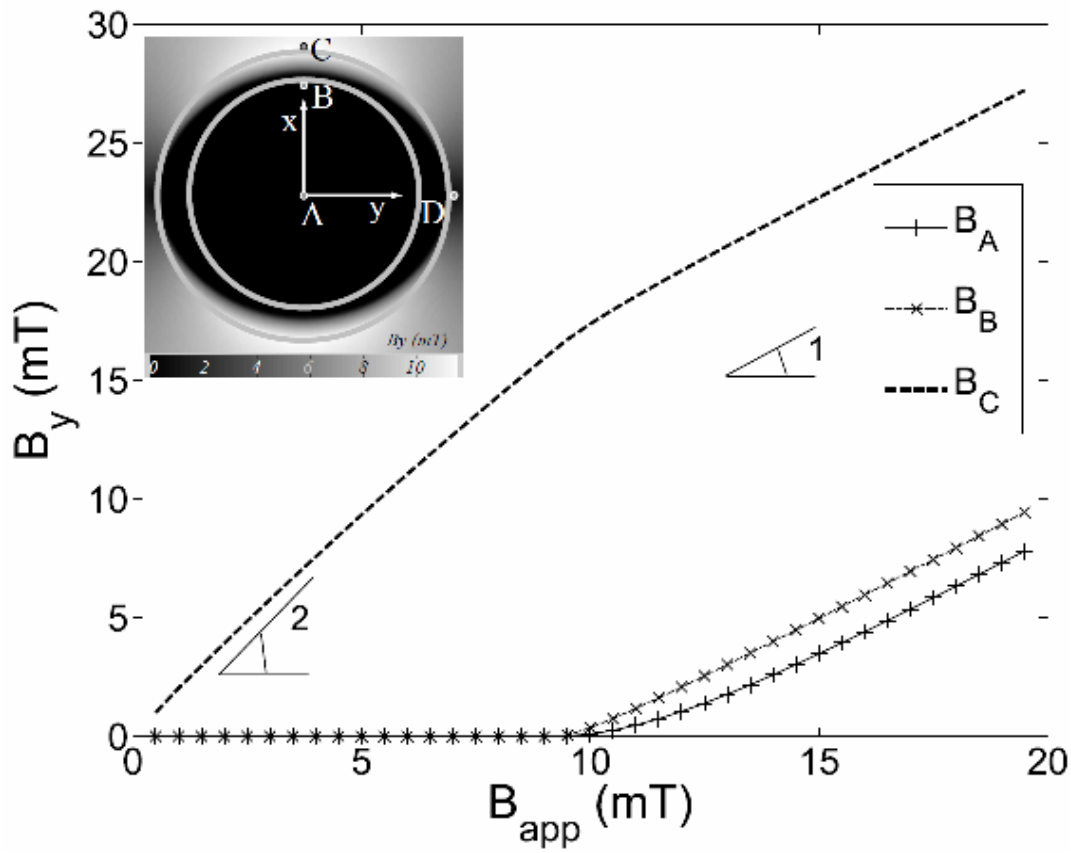

Figure 10. Transverse component of the local magnetic flux density, B_y, as a function of the applied magnetic field at point A (B_{in}), at point B (B_{inner}), and at point C (B_{outer}), for a constant J_c = 1000 A/cm² and in the transverse magnetic field configuration.
Inset: Distribution of the transverse component of the local magnetic flux density, B_y, for a transverse applied magnetic field $\mu_0 H_{app}$ = 6.6 mT.

Once the superconductor is fully penetrated, the outer magnetic field also increases proportionally to B_{app}, the slope tends to unity. The magnetic field at point B increases linearly with B_{app}. As the magnetic field at the centre of the tube (at point A) results from the flux penetration contributions over all the azimuthal angles, it thus increases less rapidly than B_{outer} for small B_{app} until the entire inner border is penetrated and the magnetic field increases at the rate of dB_{app}/dt.

These results show that a simple model based on the discussion of the demagnetizing factor can be used to reproduce the local values of the magnetic flux density below and above B_{lim}.

In the case of a field-dependent critical current density following the Kim model of equation (8), the flux profile within the superconductor thickness is no longer linear as was the case for a constant J_c, but presents instead a negative second derivative along x. This result arises from a current density increasing from the outer radius to the inner radius (figure 11). As a result, the gradient of B_y increases towards the inner border of the superconducting tube and the magnetic flux enters more rapidly into the tube so that the slope of the curve $B_{inner}(B_{app})$ is greater than unity as opposed to the case of a field-independent J_c.

6. Conclusions

In this work, we have studied the magnetic shielding behaviour of superconducting hollow cylinders both (i) experimentally by applying transverse and axial magnetic fields with a constant sweep rate between 10 μT/s and 10 mT/s and (ii) theoretically for the same magnetic field configurations by using a method involving a non-linear $\boldsymbol{E}(\boldsymbol{J})$ constitutive law and a field-dependent critical current density.

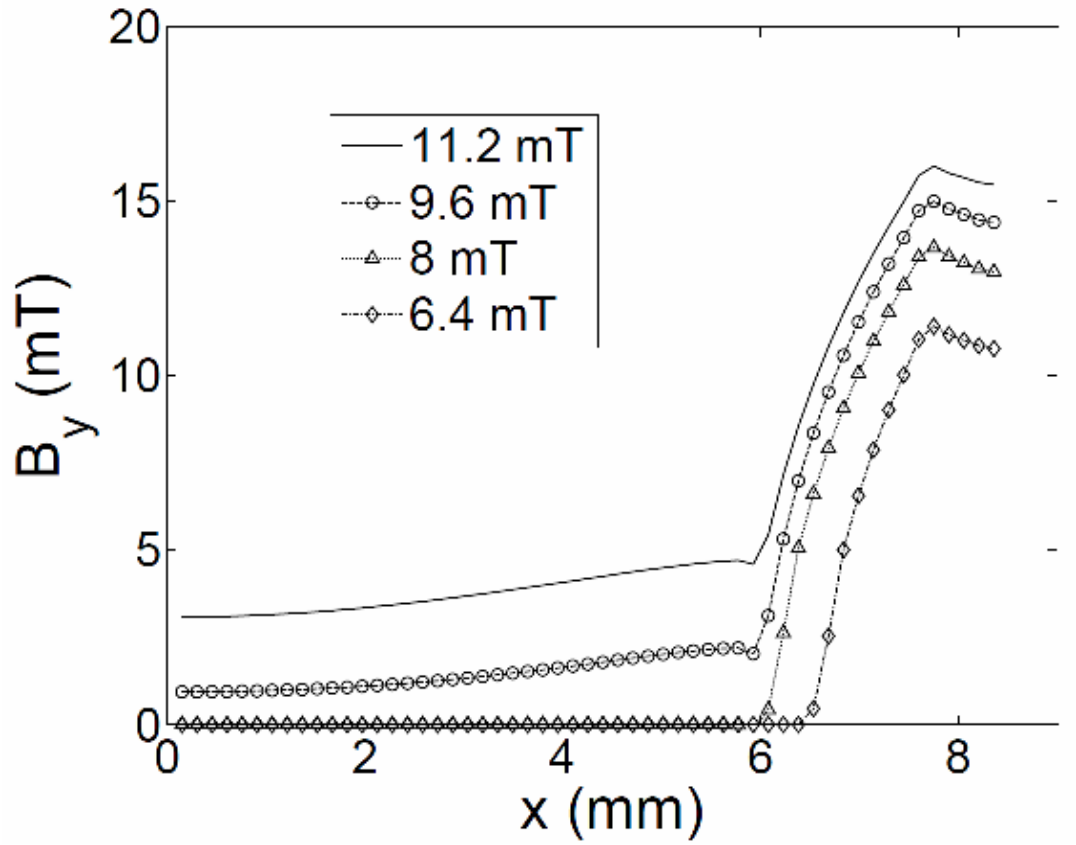

Figure 11. Distribution of the transverse component of the local magnetic flux density, B_y, along x for a field-dependent J_c (J_{c0} = 4000 A/cm², B_1 = 2 mT) and in the transverse magnetic field configuration.

From the experiments on a Pb-doped Bi-2223 tube at 77 K, the threshold magnetic field, B_{lim}, was determined and the sweep rate dependence of B_{lim} was pointed out. We found that its sweep rate dependence can be described by a power law with large n'-exponents whose values are of the same order of magnitude for both configurations.

The analysis of the constitutive laws and the numerical results showed a link between the n-exponent of the $E(J)$ power law and the n'-exponent of the $dB_{app}/dt(B_{lim})$ relationship due to the field dependence of the critical current density in both axial and transverse magnetic field configurations. With numerical simulations, we show that, for a constant J_c, n, and n' are equal. On the other hand, in the case of a field-dependent J_c, the exponents are related by the equation $n' = n\,(1+\gamma)$ where γ is the exponent of a negative power law $J_c(B)$.

We suggested a method to determine a single set of intrinsic parameters (J_{c0}, B_1, n) describing the superconducting behaviour of the material in both axial and transverse configurations. The method is based on modelling experimental results, starting from initial values of a simple one-dimensional model. The method has been applied with success to our measurements and the resulting parameters for the sample Bi-2223 hollow cylinder at 77 K are given as J_{c0} = 4000 A/cm², B_1 = 2 mT and n = 29. The numerical value of n' matches that obtained by fits to experimental data in both axial and transverse magnetic field configurations.

From a practical point of view, for known parameters of a superconducting material, the modelling can then be extended outside the frequency window attainable experimentally or can be used for designing magnetic shields of large dimensions.

Both experiment and simulation results have confirmed the importance of the magnetic field dependence of the critical current density on the shielding properties of superconducting hollow cylinders. The sweep rate dependence of B_{lim} is ruled by the intrinsic n-exponent of the $E(J)$ power law but the complex profiles of the flux penetration induced by the $J_c(B)$ dependence has to be taken into account in order to properly describe the penetration of the flux inside the hollow cylinder for both axial and transverse magnetic field configurations.

Finally, we showed that a simple model based on the demagnetizing effects is sufficient to explain the modification of the applied magnetic field surrounding the superconducting tube when the magnetic field is applied transversally. The local magnification of the applied magnetic field at the sides of the tube leads to an anisotropy of the flux front inside the thickness of the tube and then to a lower value of B_{lim} in the transverse configuration than in the axial configuration.

Acknowledgments.
We are particularly grateful to the Royal Military Academy, FNRS and ULg for cryofluid, equipment and travel grants.

References

[1] Pavese F 1998 *Handbook of Applied Superconductivity* (IoP Publishing) 1461
[2] Kamiya K, Warner B and DiPirro M 2001 *Cryogenics* **41** 401
[3] Ohta H et al 1999 *IEEE Trans. Appl. Supercond.* **9** 4073
[4] Pizzella V, Della Penna S, Del Gratta C and Luca Romani G 2001 *Supercond. Sci. Technol.* **14** R79
[5] Holmes J. J 2008 *Synthesis Lectures on Computational Electromagnetics* **3** 1
[6] Frankel D 1979 *IEEE Trans. Magn.* **MAG-15** 1349
[7] Plechacek V, Hejtmanek J, Sedmidubsky D, Knizek K, Pollert E, Janu Z and Tichy R 1995 *IEEE Trans. Appl. Supercond.* **5** 528
[8] Bean C 1962 *Phys. Rev. Lett.* **8** 250
[9] Bhagwat K V and Chaddah P 1991 *Phys. Rev. B* **44** 6950
[10] Fagnard J-F, Denis S, Lousberg G, Dirickx M, Ausloos M, Vanderheyden B and Vanderbemden P 2009 *IEEE Trans. Appl. Supercond.* in press
[11] Campbell A 1991 *IEEE Trans. Magn.* **27** 1660
[12] Cesnak L, Gömöry F, Kovác P, Souc J, Fröhlich K, Melisek T, Hilscher G, Puttner M and Holubar T 1996 *Applied Superconductivity* **4** 277
[13] Brandt E H 1997 *Phys. Rev. B* **55** 14513
[14] Brandt E H 1998 *Phys. Rev. B* **58** 6506
[15] Brandt E H 1996 *Phys. Rev. B* **54** 4246
[16] Amemiya N, Miyamoto K, Banno N and Tsukamoto O 1997 *IEEE Trans. Appl. Supercond.* **7** 2110
[17] Bossavit A 1994 *IEEE Trans. Magn.* **30** 3363
[18] Hong Z, Campbell A M and Coombs T. A 2006 *Supercond. Sci. Technol.* **19** 1246
[19] Vanderbemden P, Hong Z, Coombs T A, Denis S, Ausloos M, Schwartz J, Rutel I B, Babu N H, Cardwell D A and Campbell A M 2007 *Phys. Rev. B* **75** 174515
[20] Sirois F, Cave J and Basile-Bellavance Y 2007 *IEEE Trans. Appl. Supercond.* **17** 3652
[21] Duron J, Grilli F, Dutoit B and Stavrev S 2004 *Physica C* **401** 231
[22] Gomory F, Vojenciak M, Pardo E and Souc J 2009 *Supercond. Sci. Technol.* **22** 034017
[23] Lousberg G. P, Ausloos M, Geuzaine C, Dular P, Vanderbemden P and Vanderheyden V 2009 *Supercond. Sci. Technol.* in press
[24] Masson P, Netter D, Leveque J and Rezzoug A 2001 *IEEE Trans. Appl. Supercond.* **11** 2248
[25] Badia-Majos A 2006 *Am. J. Phys.* **74** 1136
[26] Denis S, Dusoulier L, Dirickx M, Vanderbemden P, Cloots R, Ausloos M and Vanderheyden B 2007 *Supercond. Sci. Technol.* **20** 192
[27] Carr W. J 2001 *AC Loss and Macroscopic Theory of Superconductors* (CRC Press) 212
[28] Zolotovitskii A B, Reiderman A F, Glazer B. A, Lappo I. S, Lyakin V V and Raevskii V Y 1991 *Superconductivity* **4** 810
[29] Zhilichev Y N 1997 *IEEE Trans. Appl. Supercond.* **7** 3874
[30] Zhilichev Y N 2000 *IEEE Trans. Appl. Supercond.* **10** 1657
[31] Hong Z, Vanderbemden P, Pei R, Jiang Y, Campbell A and Coombs T 2008 *IEEE Trans. Appl. Supercond.* **18** 1561
[32] Pardo E, Sanchez A and Navau C 2003 *Phys. Rev. B* **67** 104517
[33] Matsuba H, Yahara A and Irisawa D 1992 *Supercond. Sci. Technol.* **5** S432
[34] Mikitik G P and Brandt E H 2005 *Phys. Rev. B* **71** 012510

[35] Karmakar D and Bhagwat K 2003 *Physica C* **398** 20
[36] Denis S, Dirickx M, Vanderbemden P, Ausloos M and Vanderheyden B 2007 *Supercond. Sci. Technol.* **20** 418
[37] Kim Y, Hempstead C and Strnad A 1962 *Phys. Rev. Lett.* **9** 306
[38] Denis S 2007 Magnetic shielding with high-temperature superconductors *PhD Thesis* University of Liège
[39] Yamasaki H and Mawatari Y 2000 *Supercond. Sci. Technol.* **13** 202
[40] Osborn J A 1945 *Phys. Rev.* **67** 351
[41] Chen D X, Brug J A and Goldfarb R B 1991 *IEEE Trans. Magn.* **27** 3601
[42] Chen D X, Pardo E and Sanchez A 2001 *IEEE Trans. Magn.* **37** 3877